

Hole Detrapping-Type Persistent Phosphors of RE_2O_3 (RE = La, Gd, Y, Lu) Doped with Eu^{3+} - Pr^{3+} and Eu^{3+} - Tb^{3+}

Hashimoto, Atsunori; Ueda, Jumpei; Aoki, Yasushi; Dorenbos, Pieter; Tanabe, Setsuhisa

DOI

[10.1021/acs.jpcc.3c03251](https://doi.org/10.1021/acs.jpcc.3c03251)

Publication date

2023

Document Version

Final published version

Published in

Journal of Physical Chemistry C

Citation (APA)

Hashimoto, A., Ueda, J., Aoki, Y., Dorenbos, P., & Tanabe, S. (2023). Hole Detrapping-Type Persistent Phosphors of RE_2O_3 (RE = La, Gd, Y, Lu) Doped with Eu^{3+} - Pr^{3+} and Eu^{3+} - Tb^{3+} . *Journal of Physical Chemistry C*, 127(32), 15611-15619. <https://doi.org/10.1021/acs.jpcc.3c03251>

Important note

To cite this publication, please use the final published version (if applicable). Please check the document version above.

Copyright

Other than for strictly personal use, it is not permitted to download, forward or distribute the text or part of it, without the consent of the author(s) and/or copyright holder(s), unless the work is under an open content license such as Creative Commons.

Takedown policy

Please contact us and provide details if you believe this document breaches copyrights. We will remove access to the work immediately and investigate your claim.

Green Open Access added to TU Delft Institutional Repository

'You share, we take care!' - Taverne project

<https://www.openaccess.nl/en/you-share-we-take-care>

Otherwise as indicated in the copyright section: the publisher is the copyright holder of this work and the author uses the Dutch legislation to make this work public.

Hole Detrapping-Type Persistent Phosphors of RE₂O₂S (RE = La, Gd, Y, Lu) Doped with Eu³⁺–Pr³⁺ and Eu³⁺–Tb³⁺

Atsunori Hashimoto,¹ Jumpei Ueda,^{*1} Yasushi Aoki, Pieter Dorenbos, and Setsuhisa Tanabe



Cite This: *J. Phys. Chem. C* 2023, 127, 15611–15619



Read Online

ACCESS |



Metrics & More

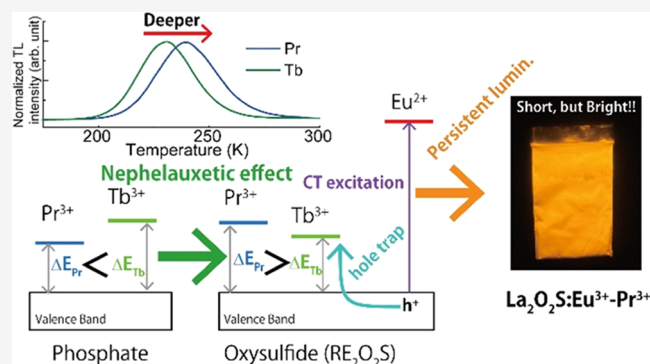


Article Recommendations



Supporting Information

ABSTRACT: RE₂O₂S:Eu³⁺–Ln³⁺ (RE = La, Gd, Y, Lu; Ln = Pr, Tb) samples were prepared by a solid-state reaction method to develop new red persistent phosphors and to demonstrate the hole detrapping mechanism. All Eu³⁺-singly doped RE₂O₂S show very weak thermoluminescence (TL) glow peaks, while by codoping Pr³⁺ or Tb³⁺ ions, additional strong TL peaks were observed. In the TL spectra and persistent luminescence (PersL) spectra, only Eu³⁺ luminescence lines were observed, but there was no Pr³⁺ and Tb³⁺ luminescence. From the PersL excitation spectra, it is found that PersL is caused after excitation to the charge transfer state of Eu²⁺–S[–] in which the hole is in the valence band. These results show that Eu³⁺ acts as a recombination center and Pr³⁺ and Tb³⁺ ions act as hole trap centers. The deeper hole trap depth of Pr³⁺ than that of Tb³⁺ and the RE dependence of hole trap depth are explained using a vacuum referred binding energy diagram considering the nephelauxetic effect. La₂O₂S:Eu³⁺–Pr³⁺ was the best composition among the samples as a persistent phosphor at ambient temperature, showing strong red persistent luminescence in a short time range (>100 mcd/m² for a few seconds).



1. INTRODUCTION

Persistent phosphors, which show continuing luminescence even after the ceasing of excitation light, have been widely used as luminous paint in many products such as an emergency sign, a dial plate of a watch, etc.^{1,2} In 1993, Nemoto company developed the brightest and longest green persistent phosphor, SrAl₂O₄:Eu²⁺–Dy³⁺, and published a paper in 1996.³ In this phosphor, the persistent luminescence is caused by the 4f⁶5d¹ → 4f⁷ transition of Eu²⁺. At that time, the persistent luminescence mechanism was not well understood and a hole transfer model (Eu²⁺–Dy³⁺ ⇌ Eu⁺–Dy⁴⁺) was proposed. Nowadays, it is considered that the persistent luminescence in SrAl₂O₄:Eu²⁺–Dy³⁺ is caused by the electron transfer process (Eu²⁺–Dy³⁺ ⇌ Eu³⁺–Dy²⁺).^{4,5}

On the other hand, Nichia company successfully developed a bright red persistent phosphor, Y₂O₂S:Eu³⁺–Ti⁴⁺–Mg²⁺, in 1998.⁶ The persistent luminescence center is Eu³⁺, which shows strong red 4f–4f luminescence (⁵D₀ → ⁷F₂). Opposite to SrAl₂O₄:Eu²⁺–Dy³⁺, it is suggested that Y₂O₂S:Eu³⁺–Ti⁴⁺–Mg²⁺ persistent luminescence is caused by the hole transfer process (Eu³⁺ ⇌ Eu²⁺ + h⁺), although the hole trapping center is not identified.⁷ To develop a new persistent phosphor based on the hole transfer model and to demonstrate its persistent luminescence mechanism in Eu³⁺-doped rare earth oxysulfide compounds, hole traps and their trap depth must be managed. The vacuum referred binding energy (VRBE) diagram of RE₂O₂S (RE = La, Gd, Y, Lu), demonstrates a possibility that Pr³⁺ and Tb³⁺ can act as hole traps.⁷ If Pr³⁺ and Tb³⁺ ions act

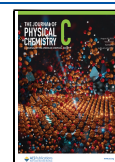
as traps in RE₂O₂S:Eu³⁺ red phosphors, the mechanism of persistent luminescence is supported to be based on the hole transfer model. In the hole transfer model, the hole trap depth can be engineered by either selecting Pr³⁺ or Tb³⁺ or by altering the top of valence band energy by changing the type of host compound rare earth ion. Also, recently, strong mechanoluminescence has been reported in RE₂O₂S:Ln³⁺ (RE = Y, Lu, La, or Gd; Ln = Eu, Pr, Nd, Sm, Tb, Dy, Ho, Er, Tm, or Yb).⁸ Thus, it is important to investigate carrier trapping and detrapping in RE₂O₂S:Ln³⁺.

In this study, Eu³⁺–Ln³⁺ (Ln = Pr and Tb)-codoped RE₂O₂S (RE = La, Gd, Y, Lu) red persistent phosphors were prepared and their optical properties were investigated. From the results of thermoluminescence and persistent luminescence measurements, it is successfully demonstrated that Pr³⁺ and Tb³⁺ ions act as hole traps. Also, variations in hole trap depths by Pr³⁺ and Tb³⁺ ions in the RE₂O₂S host were explained using a newly constructed vacuum referred binding energy diagram that takes the nephelauxetic effect into account.

Received: May 16, 2023

Revised: July 3, 2023

Published: July 26, 2023



2. EXPERIMENTAL PROCEDURE

$\text{RE}_{1.99}\text{Eu}_{0.01}\text{O}_2\text{S}$ and $\text{RE}_{1.988}\text{Eu}_{0.01}\text{Ln}_{0.002}\text{O}_2\text{S}$ (RE = La, Gd, Y, Lu; Ln = Pr, Tb) were prepared by a solid-state reaction method. La_2O_3 , Gd_2O_3 , Y_2O_3 , Lu_2O_3 , Eu_2O_3 , Pr_6O_{11} , Tb_4O_7 , and S were used as raw materials. In order to prevent oxidation, an excess amount of sulfur was added. Also, Na_2CO_3 and K_3PO_4 were used to facilitate the solid-state reaction. These chemicals were mixed by ball milling and sintered at 1200 °C for 4 h in air. The obtained materials were washed with deionized water several times to remove remnants. The crystal phases of samples were analyzed by an XRD measurement system (XRD-6100, Shimadzu). Photoluminescence (PL) and photoluminescence excitation (PLE) spectra were measured by a self-built spectrometer; monochromatic excitation light was generated by a 500 W Xe short arc lamp (OPM2-502XQ, Ushio Inc.) and a double monochromator setup using two single monochromators (SpectraPro-300i, Acton Research Corporation) and luminescence was detected by a photomultiplier tube (R10699, Hamamatsu Photonics) equipped with a single monochromator (SP-2300i, Princeton Instruments). The measured PLE spectra were calibrated by a photon flux spectrum of an excitation light source, which was measured using a standard Si (S1337-1010BQ, Hamamatsu Photonics). The PL spectra were calibrated by a standard halogen lamp (DH-2000CAL, Ocean Photonics) to the photon flux spectrum. Thermoluminescence (TL) glow curves were measured using a photomultiplier tube, PMT (R3896, Hamamatsu Photonics) with a bandpass filter of 640 nm with 100 nm FWHM. The samples were fixed into a cryostat (VPF-800, Janis) to control the temperature. The samples were charged by UV excitation (250–400 nm) from a 300 W Xe lamp (MAX-302, Asahi Spectra) at 80 K for 10 min and kept for 10 min after ceasing excitation at the same temperature. The sample was then heated with a heating rate of 10 K/min up to 400 K. The TL spectra were measured simultaneously by a Si CCD spectrometer (QE65-Pro, Ocean Optics). Persistent luminescence (PersL) spectra were detected by a Si CCD spectrometer (PMA-12, Hamamatsu Photonics). PersL decay curves were measured by a luminance meter (LS-100, KONICA MINOLTA) after UV irradiation. For PersL excitation (PersLE) spectra, the sample was irradiated for 5 min by monochromatic light, and 1 min after stopping irradiation, PersL spectra were measured by a spectrophotometer (RF-5000, Shimadzu).

3. RESULTS

3.1. Crystal Structure. Figure 1 shows the X-ray diffraction (XRD) patterns of Eu^{3+} -doped $\text{RE}_2\text{O}_2\text{S}$ ($\text{RE}_2\text{O}_2\text{S}:\text{Eu}^{3+}$; RE = La, Gd, Y, Lu). The observed XRD patterns of Eu^{3+} -doped $\text{La}_2\text{O}_2\text{S}$, $\text{Gd}_2\text{O}_2\text{S}$, $\text{Y}_2\text{O}_2\text{S}$, and $\text{Lu}_2\text{O}_2\text{S}$ correspond to the reference XRD patterns of $\text{RE}_2\text{O}_2\text{S}$ (RE = La, Gd, Y, Lu) in the ICDD (International Centre for Diffraction Data) database with card numbers #01-071-2098, #01-079-5662, #00-024-1424, and #00-026-1445, respectively. Thus, all samples are identified as a single crystalline phase of $\text{RE}_2\text{O}_2\text{S}$ (RE = La, Gd, Y, Lu) with the space group of $P\bar{3}m1$. The observed XRD peaks are shifted to the higher diffraction angle in the order of $\text{La}_2\text{O}_2\text{S}$, $\text{Gd}_2\text{O}_2\text{S}$, $\text{Y}_2\text{O}_2\text{S}$, and $\text{Lu}_2\text{O}_2\text{S}$ because the cation size of RE ion becomes smaller in the same order. Consequently, the lattice constant decreases in the order of $\text{La}_2\text{O}_2\text{S}$, $\text{Gd}_2\text{O}_2\text{S}$, $\text{Y}_2\text{O}_2\text{S}$, and $\text{Lu}_2\text{O}_2\text{S}$.

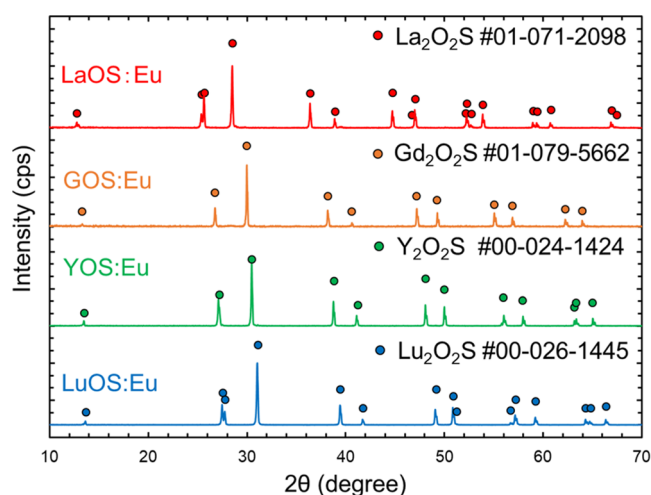


Figure 1. X-ray diffraction (XRD) patterns of $\text{RE}_2\text{O}_2\text{S}:\text{Eu}^{3+}$ (RE = La, Gd, Y, Lu).

3.2. PL and PLE Properties. Figure 2 shows the PL spectra of $\text{RE}_2\text{O}_2\text{S}:\text{Eu}^{3+}$ (RE = La, Gd, Y, Lu). All samples show strong red luminescence mainly due to the typical Eu^{3+} 4f–4f luminescence ($^5\text{D}_0 \rightarrow ^7\text{F}_2$) at around 625 nm. The peak wavelengths of $^5\text{D}_0 \rightarrow ^7\text{F}_2$ in $\text{La}_2\text{O}_2\text{S}$, $\text{Gd}_2\text{O}_2\text{S}$, $\text{Y}_2\text{O}_2\text{S}$, and $\text{Lu}_2\text{O}_2\text{S}$ were 624.6, 626.4, 627.0, and 627.6 nm, respectively, at ambient temperature. In addition to the $^5\text{D}_0 \rightarrow ^7\text{F}_1$ luminescence lines from 590 to 720 nm, several PL peaks were observed in the range from 450 to 575 nm in the $\text{La}_2\text{O}_2\text{S}$, $\text{Gd}_2\text{O}_2\text{S}$, $\text{Y}_2\text{O}_2\text{S}$, and $\text{Lu}_2\text{O}_2\text{S}$ samples. However, for $\text{La}_2\text{O}_2\text{S}:\text{Eu}^{3+}$, the luminescence peaks in the range from 450 to 520 nm are almost quenched at ambient temperature. These PL peaks can be attributed to $^5\text{D}_1 \rightarrow ^7\text{F}_1$ and $^5\text{D}_2 \rightarrow ^7\text{F}_1$ luminescence, as shown in Figure 2.

In the PLE spectra, sharp lines at around 395, 470, 530, and 580 nm and two broadbands in the range between 250 and 290 nm and between 290 and 400 nm were observed. The sharp lines are attributed to 4f–4f transitions of Eu^{3+} from $^7\text{F}_0$ to $^5\text{L}_6$, $^5\text{D}_2$, $^5\text{D}_1$, and $^5\text{D}_0$. The broadband in the longer wavelength range originates from electron transfer from the valence band to Eu^{3+} , which is called the charge transfer (CT) band. The broadband in the shorter wavelength at around 270 nm originates from the host exciton creation bands. The energy of the CT band and the host exciton band varied depending on the rare earth ion of the host compound. To clarify the host exciton energy and the CT energy in each host compound, the PLE spectra from VUV to UV were also measured at 15 K (see Figure S1 in the Supporting Information). The host exciton energy is shifted to higher energy in the order of $\text{La}_2\text{O}_2\text{S}$ (4.62 eV), $\text{Gd}_2\text{O}_2\text{S}$ (4.66 eV), $\text{Y}_2\text{O}_2\text{S}$ (4.81 eV), and $\text{Lu}_2\text{O}_2\text{S}$ (5.19 eV). The exciton creation energy seems to be very high only for $\text{Lu}_2\text{O}_2\text{S}:\text{Eu}^{3+}$, although the exciton creation energy of $\text{Lu}_2\text{O}_2\text{S}:\text{Eu}^{3+}$ at room temperature is similar to other $\text{RE}_2\text{O}_2\text{S}$ compounds (Figure 2). Compared with the PLE spectra of $\text{Lu}_2\text{O}_2\text{S}:\text{Eu}^{3+}$ in the VUV region at 300 and 15 K (Figure S2), the spectral shape is dramatically changed. Because the $\text{Lu}_2\text{O}_2\text{S}$ is a mixed anion compound, the host exciton absorption may occur from oxide 2p and sulfide 3p orbitals. At 15 K, the energy transfer from the exciton absorption due to $\text{S}(3\text{p})\text{--Lu}(5\text{d})$ to Eu^{3+} may not take place efficiently in $\text{Lu}_2\text{O}_2\text{S}:\text{Eu}^{3+}$ (Figure S2). Consequently, the host excitation energy at 15 K was overestimated in $\text{Lu}_2\text{O}_2\text{S}$. Thus, the host exciton energy of 4.82 eV, which was estimated from the

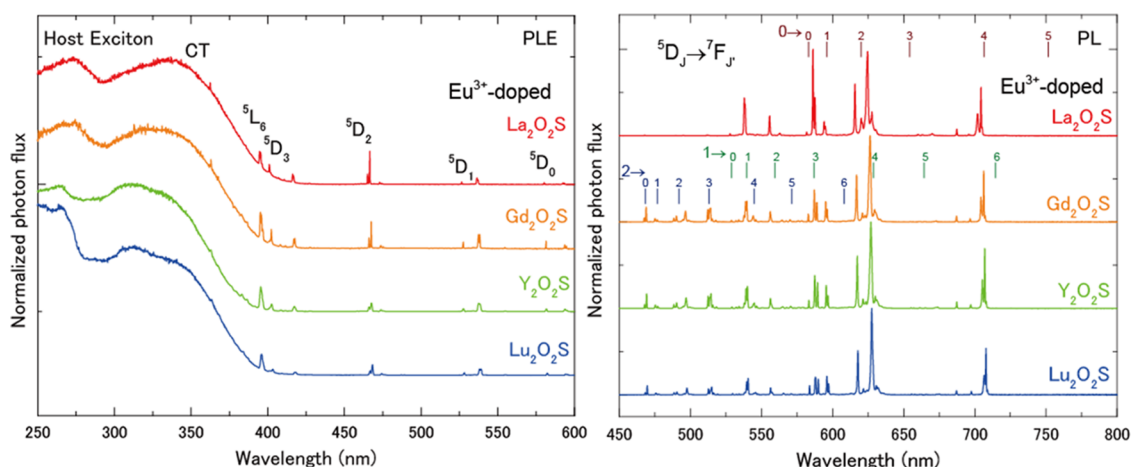


Figure 2. (a) PLE and (b) PL spectra at room temperature of RE₂O₂S:Eu³⁺ (RE = La, Gd, Y, Lu).

exciton peak at room temperature with a correction of 0.15 eV by the temperature effect, was used only for Lu₂O₂S.

3.3. TL and PersL Properties. Figure 3 shows TL glow curves of La₂O₂S:Eu³⁺ and La₂O₂S:Eu³⁺–Ln³⁺ (Ln = Pr, Tb).

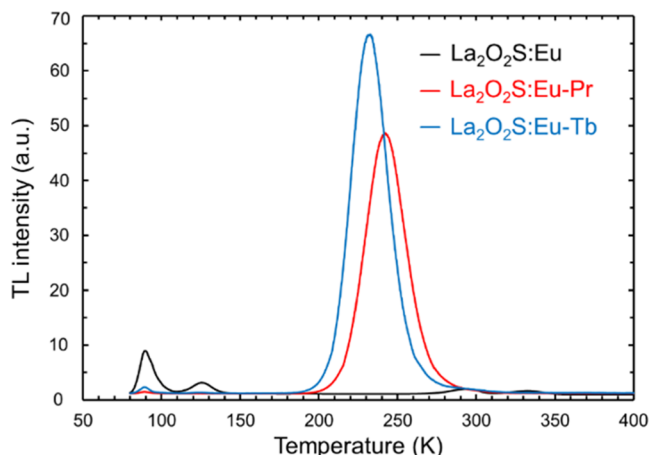


Figure 3. TL glow curves of La₂O₂S:Eu³⁺, La₂O₂S:Eu³⁺–Ln³⁺ (Ln = Pr, Tb) at a heating rate of 10 K/min after UV (250–400 nm) irradiation for 10 min.

By codoping with Pr³⁺ and Tb³⁺, additional strong TL peaks were observed. The TL peak temperatures of La₂O₂S:Eu³⁺–Pr³⁺ and La₂O₂S:Eu³⁺–Tb³⁺ are 242 and 233 K, respectively. The additional TL peaks by codoping with Pr³⁺ and Tb³⁺ were also observed in other RE₂O₂S hosts (see Figure S3–S5 in the Supporting Information). The TL glow curves in RE₂O₂S:Eu³⁺–Ln³⁺ (RE = La, Gd, Y, Lu; Ln = Pr, Tb) are summarized in the series of Pr³⁺ and Tb³⁺ codopants, as shown in Figure 4a,b, respectively. The TL glow peak is shifted by varying the rare earth ion of host compounds. The main TL glow peak temperature in La₂O₂S is the highest, followed by Y₂O₂S, Gd₂O₂S, and Lu₂O₂S in both series of RE₂O₂S:Eu³⁺–Pr³⁺ and RE₂O₂S:Eu³⁺–Tb³⁺. The TL glow peak temperatures for RE₂O₂S:Eu³⁺–Ln³⁺ (RE = La, Gd, Y, Lu; Ln = Pr, Tb) are listed in Table 1. When we compare the original TL glow peak intensity, the La₂O₂S and Y₂O₂S hosts show better performance than Gd₂O₂S and Lu₂O₂S in both Pr³⁺- and Tb³⁺-codoped ones (see Figures 3 and S3–S5).

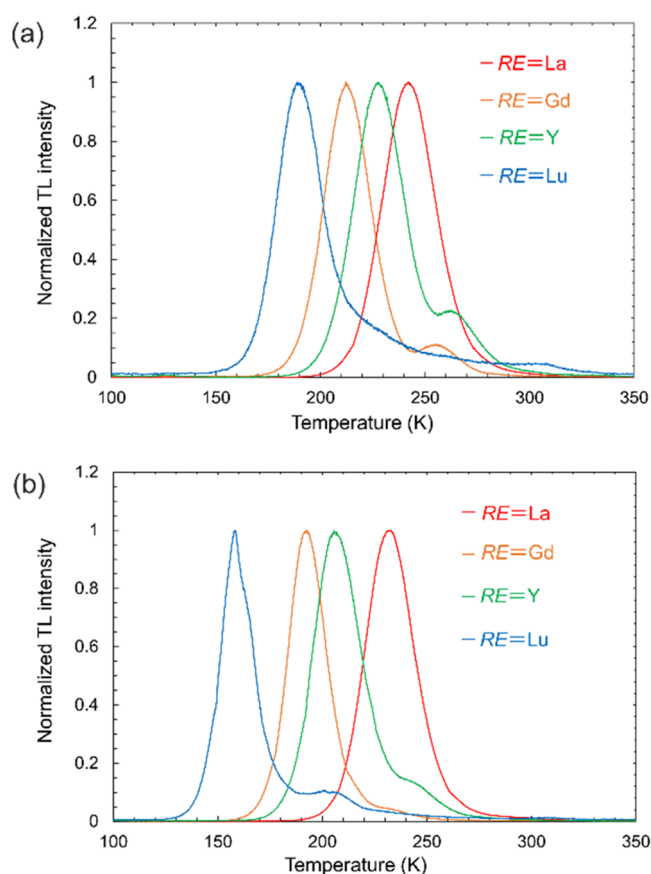


Figure 4. TL glow curves of RE₂O₂S:Eu³⁺ (RE = La, Gd, Y, Lu) (a) with the Pr³⁺ codopant and (b) with the Tb³⁺ codopant at a heating rate of 10 K/min after UV (250–400 nm) irradiation for 10 min.

From the well-known equation for the TL glow curve caused by first-order kinetics carrier transportation as presented by Randall and Wilkins,^{9,10} one can derive¹¹

$$\frac{\beta E^{\text{trap}}}{kT_m^2} = s \cdot \exp\left(-\frac{E^{\text{trap}}}{kT_m}\right) \quad (1)$$

Here, β is the heating rate (K/s), E^{trap} is the trap depth, k is the Boltzmann constant, T_m is the maximum temperature of the TL glow peak, and s is the frequency factor. Thus, from the obtained TL glow peak temperature, the trap depths can be

Table 1. Frequency Factor (s),⁷ Temperature Maximum (T_m) of TL Glow Curves at a Heating Rate of 10 K/min, and the Derived Trap Depth (E^{trap}) of $\text{RE}_2\text{O}_2\text{S}:\text{Eu}^{3+}-\text{Ln}^{3+}$ (RE = La, Gd, Y, Lu, Ln = Pr, Tb)

| | frequency factor (s^{-1}) ⁷ | T_m (K) | | E^{trap} (eV) | |
|---------|--|-----------|-----|------------------------|------|
| | | Pr | Tb | Pr | Tb |
| RE = La | 1.1×10^{13} | 242 | 233 | 0.70 | 0.68 |
| RE = Gd | 1.3×10^{13} | 212 | 192 | 0.62 | 0.56 |
| RE = Y | 1.3×10^{13} | 228 | 206 | 0.66 | 0.60 |
| RE = Lu | 1.4×10^{13} | 189 | 158 | 0.55 | 0.46 |

estimated by assuming the frequency factor. The frequency factors were reported in ref 7, as shown in column 2 of Table 1. The calculated trap depths in $\text{RE}_2\text{O}_2\text{S}:\text{Eu}^{3+}-\text{Ln}^{3+}$ (RE = La, Gd, Y, Lu; Ln = Pr, Tb) are shown in Table 1. The trap depth of the main TL glow peak in RE = La is the deepest, followed by RE = Y, Gd, and Lu in the series of both $\text{RE}_2\text{O}_2\text{S}:\text{Eu}^{3+}-\text{Pr}^{3+}$ and $\text{RE}_2\text{O}_2\text{S}:\text{Eu}^{3+}-\text{Tb}^{3+}$.

Figure 5a and b show the luminescence wavelength–temperature ($\lambda_{\text{em}}-T$) contour plots of the TL intensity of $\text{La}_2\text{O}_2\text{S}:\text{Eu}^{3+}-\text{Ln}^{3+}$ (Ln = Pr, Tb). The observed TL peaks originate only from Eu^{3+} 4f–4f transition. No TL emissions from Pr^{3+} and Tb^{3+} were observed in the temperature range from 100 to 400 K.

Figure 6a shows the PersL spectra of $\text{La}_2\text{O}_2\text{S}:\text{Eu}^{3+}$ and $\text{La}_2\text{O}_2\text{S}:\text{Eu}^{3+}-\text{Ln}^{3+}$ (Ln = Pr, Tb). These samples showed red persistent luminescence. By codoping the lanthanide ions, the intensities of persistent luminescence become stronger than those of Eu^{3+} singly doped $\text{La}_2\text{O}_2\text{S}$. In these samples, no persistent luminescence from Pr^{3+} and Tb^{3+} was observed similar to TL spectra in Figure 5, which indicates that only the Eu^{3+} ions act as a recombination center. In the samples of RE = Gd, Y, and Lu, PersL cannot be detected by the Si CCD at ambient temperature because of too shallow trap depths. Figure 6b shows the PersL decay curves of the $\text{La}_2\text{O}_2\text{S}:\text{Eu}^{3+}$ and $\text{La}_2\text{O}_2\text{S}:\text{Eu}^{3+}-\text{Ln}^{3+}$ (Ln = Pr, Tb) samples. By the addition of the codopant, the luminance is enhanced compared with Eu^{3+} singly doped $\text{La}_2\text{O}_2\text{S}$. The persistent luminescence duration of $\text{La}_2\text{O}_2\text{S}:\text{Eu}^{3+}-\text{Pr}^{3+}$ is the longest in these $\text{La}_2\text{O}_2\text{S}$ -based samples and the duration time is 60 s until the luminance drops 2 mcd/m².

Figure 7 shows the PersLE spectra of $\text{La}_2\text{O}_2\text{S}:\text{Eu}^{3+}-\text{Pr}^{3+}$. Two excitation bands were observed. The PersLE band at 230 nm is attributed to the host exciton creation band and another band at 380 nm is the CT band of Eu^{3+} .

4. DISCUSSION

4.1. Quenching Process and Nephelauxetic Effect of Eu^{3+} Luminescence. As shown in Figure 2b, only $\text{La}_2\text{O}_2\text{S}$ does not show the luminescence from the $^5\text{D}_2$ excited state. The possible quenching processes are multiphonon relaxation, cross-relaxation, and thermally activated crossover to the CT state. The relatively low phonon energies ($\sim 500 \text{ cm}^{-1}$)¹² of the $\text{RE}_2\text{O}_2\text{S}$ compounds imply no multiphonon relaxation quenching. Also, the low Eu^{3+} concentration (0.5%) means no cross-relation quenching. However, the CT absorption edge of $\text{La}_2\text{O}_2\text{S}:\text{Eu}^{3+}$ in Figure 2a shows the longest wavelength among $\text{RE}_2\text{O}_2\text{S}:\text{Eu}^{3+}$ (RE = La, Gd, Y, and Lu), indicating that the activation energy to the CT state is small. Thus, the $^5\text{D}_2$ luminescence quenching in $\text{La}_2\text{O}_2\text{S}:\text{Eu}^{3+}$ can be caused by the CT state.

4.2. Hole Trap by Pr^{3+} and Tb^{3+} . As expected, Pr^{3+} and Tb^{3+} codoping generated additional TL glow peaks (Figures 3 and 4). The persistent luminescence (thermoluminescence) center was identified to be only Eu^{3+} based on the PersL and TL spectra (Figures 5 and 6). The Eu^{3+} persistent luminescence was caused after excitation upon the charge transfer band of Eu^{3+} and band-to-band absorption (Figure 7). These results strongly show that the persistent luminescence is caused by the hole transfer process.

When the CT band of Eu^{3+} is excited, the $\text{Eu}^{3+}-\text{S}^{2-}$ state is changed into $\text{Eu}^{2+}-\text{S}^-$ because the electron of the 3p orbital of S^{2-} is transferred to Eu^{3+} . One may equally well state that a hole is transferred from Eu^{3+} to S^{2-} , which forms the top of VB. In the hole picture model,¹³ the CT excitation is depicted by arrow 1 in Figure 8. This free hole in the valence band can be captured by Ln^{3+} (Pr^{3+} , Tb^{3+}), which then changes into a tetravalent state. The tetravalent state is known as a stable valence state for Pr and Tb in many compounds. This hole trapping process is illustrated by arrow 2 in Figure 8. On the other hand, the Eu^{3+} ion keeps the excited electron from S^{2-} through the CT absorption, which means that the Eu^{3+} ion acts as an electron trap. Thus, the valence state change of $\text{Eu}^{3+}-$

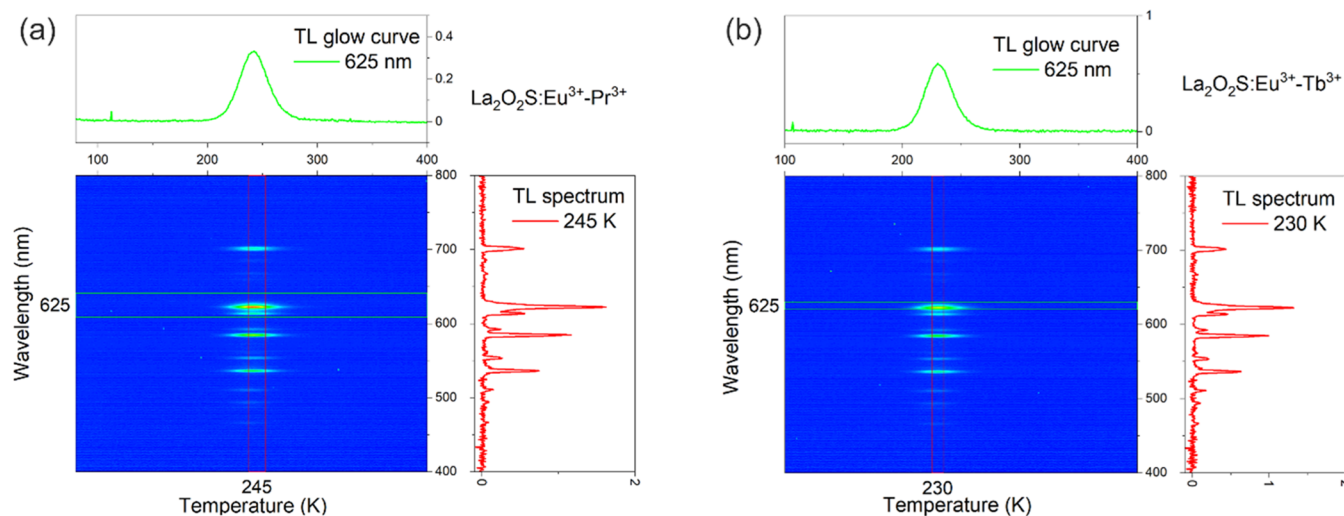


Figure 5. Emission wavelength–temperature ($\lambda_{\text{em}}-T$) contour plots of the TL intensity for (a) $\text{La}_2\text{O}_2\text{S}:\text{Eu}^{3+}-\text{Pr}^{3+}$ and (b) $\text{La}_2\text{O}_2\text{S}:\text{Eu}^{3+}-\text{Tb}^{3+}$.

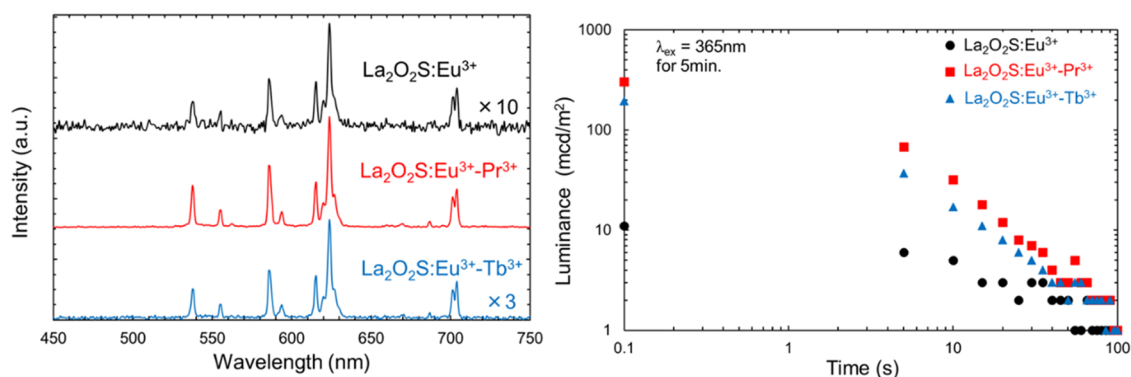


Figure 6. (a) PersL spectra and (b) PersL decay curves of La₂O₂S:Eu³⁺ and La₂O₂S:Eu³⁺-Ln³⁺ (Ln = Pr, Tb).

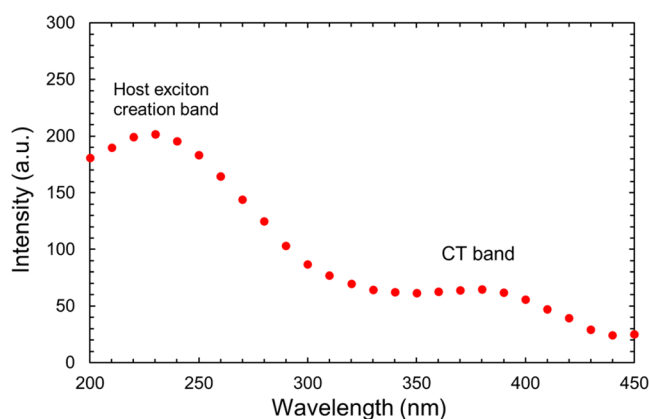


Figure 7. PersL excitation spectra of La₂O₂S:Eu³⁺-Pr³⁺.

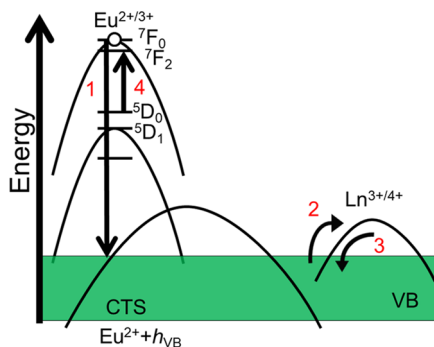


Figure 8. Persistent luminescence mechanism based on the hole picture model. (1) Excitation to the charge transfer state, (2) hole trapping, (3) hole detrapping, and (4) ⁵D₀-⁷F₂ luminescence.

Ln³⁺ ⇌ Eu²⁺-Ln⁴⁺ (Ln = Pr, Tb) is our proposed carrier trapping mechanism. So far, these kinds of valence state changes have been demonstrated using UV-vis absorption spectroscopy and X-ray absorption spectroscopy.^{5,14-17} The trapped hole by Pr³⁺ or Tb³⁺ can be released at a lower temperature than the electron from the electron-trapped Eu³⁺ (Eu²⁺). If the electron of Eu²⁺ is detrapped at a lower temperature, the Pr³⁺ and Tb³⁺ ions should be recombination centers, but the PersL of Pr³⁺ and Tb³⁺ was not observed. Thus, the hole transfer and the hole detrapping process support the fact that only Eu³⁺ shows persistent luminescence.

4.3. Hole Trap Depth in the VRBE Diagram. To understand the hole trap depth by Pr³⁺ and Tb³⁺ in RE₂O₂S, the VRBE (vacuum referred binding energy diagram) can be useful. The VRBE diagrams of RE₂O₂S were reported by Luo

et al. in 2017.⁷ Based on the VRBE in 2017, it is considered that the Tb³⁺ forms deeper hole traps compared with Pr³⁺ in all of the RE₂O₂S hosts and the hole trap depth of both Pr³⁺ and Tb³⁺ becomes deeper in the order of La₂O₂S, Gd₂O₂S, Y₂O₂S, and Lu₂O₂S with decreasing RE ionic radius, as shown in Table 2. However, the obtained trap depth in RE₂O₂S:Eu³⁺-Ln³⁺ as

Table 2. Estimated Hole Trap Depth of Pr³⁺ and Tb³⁺ in RE₂O₂S Hosts Based on the VRBE Diagram Reported in Ref 7 in eV

| | Pr ³⁺ | Tb ³⁺ |
|----------------------------------|------------------|------------------|
| La ₂ O ₂ S | 0.63 | 0.81 |
| Gd ₂ O ₂ S | 0.74 | 0.92 |
| Y ₂ O ₂ S | 0.77 | 0.95 |
| Lu ₂ O ₂ S | 0.79 | 0.97 |

shown in Table 1 does not follow this trend. The observed hole trap depth of Tb³⁺ is always shallower than that of Pr³⁺ in all of the RE₂O₂S hosts. In addition, the hole trap depth by Pr³⁺ and Tb³⁺ in La₂O₂S is the deepest and that in Lu₂O₂S is the shallowest among the RE₂O₂S hosts.

Although the typical errors in VRBE construction are several 0.1 eV, there seems to be a clear inconsistency in the trends with changing RE and between Pr³⁺ and Tb³⁺. In 2019, Dorenbos improved the model of VRBE diagram construction by considering the nephelauxetic effect on VRBE energies.¹⁸ It was found that the nephelauxetic effect may lower the right-hand branch ($n = 8-14$) of the zig-zag curves of Ln²⁺ and Ln³⁺ by several 0.1 eV with respect to the left-hand branch ($n = 1$ to 7). Here, n is the number of 4f electrons of Ln³⁺. In the RE₂O₂S hosts, an enhanced nephelauxetic effect is to be expected due to the smaller electronegativity of sulfide ($\chi_s = 2.58$) than those of pure oxide materials ($\chi_o = 3.44$). The branch lowering in the zig-zag curve of Ln³⁺ is crucial for the hole trap depth difference between Pr³⁺ and Tb³⁺.¹⁹ For instance, in the REPO₄ compounds, which show a low nephelauxetic effect by the oxygen ligand because of the strong bonding between P⁵⁺ and O²⁻, the Tb³⁺ hole trap depth is deeper than the Pr³⁺ hole trap. On the other hand, in the rare earth aluminates such as Y₃Al₅O₁₂ and GdAlO₃, which show a slightly larger nephelauxetic effect due to the weaker bonding of Al³⁺-O²⁻ than that of P⁵⁺-O²⁻, the Tb³⁺ hole trap depth is shallower than the Pr³⁺ hole trap.¹⁹ The same appears now for the oxysulfides in this work. Dorenbos introduced the nephelauxetic ratio β as a parameter to quantify the branch lowering.^{18,19} β is defined by the ratio of the Slater-Condon parameter F^2 for the lanthanides in compound A with respect

to that for lanthanides in vacuum. The β parameter is directly linked to the energy difference $\Delta E(8,2,A)$ between the VRBE of Tb^{3+} and the VRBE of Pr^{3+} .¹⁹ From the hole trap depths (Table 1), the $\Delta E(8,2,A)$ values of $\text{La}_2\text{O}_2\text{S}$, $\text{Gd}_2\text{O}_2\text{S}$, $\text{Y}_2\text{O}_2\text{S}$, and $\text{Lu}_2\text{O}_2\text{S}$ amount -0.02 , -0.06 , -0.06 , and -0.09 eV, respectively, which leads into the decreasing β parameter as 0.930, 0.927, 0.927, and 0.924, respectively. The decreasing tendency of β in the order of $\text{La}_2\text{O}_2\text{S}$, $\text{Gd}_2\text{O}_2\text{S}$, $\text{Y}_2\text{O}_2\text{S}$, and $\text{Lu}_2\text{O}_2\text{S}$ suggests that the environment at the RE site becomes more covalent. This tendency cannot be explained by the electronegativity of the RE cation, which increases from La to Lu. In this series, a smaller RE site size can increase the nephelauxetic effect due to the shorter distance with the anion.

Also, the same nephelauxetic effect is apparent in the Eu^{3+} luminescence peak position. Figure 9 shows the host rare earth

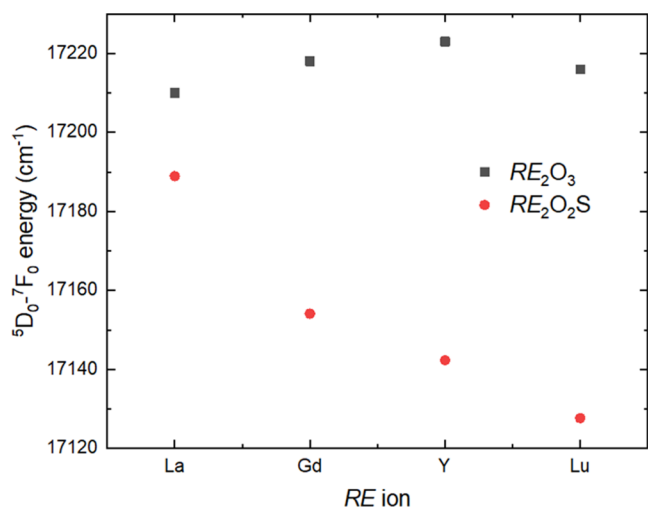


Figure 9. Host rare earth ion dependence of $\text{Eu}^{3+} : ^5\text{D}_0 - ^7\text{F}_0$ energy in $\text{RE}_2\text{O}_2\text{S}$ and RE_2O_3 .^{20,21}

ion dependence of the $\text{Eu}^{3+} : ^5\text{D}_0 - ^7\text{F}_0$ energy in $\text{RE}_2\text{O}_2\text{S}$ obtained from PL spectra in Figure 2 together with data on $\text{RE}_2\text{O}_3 : \text{Eu}^{3+}$ as a reference. For the $\text{RE}_2\text{O}_3 : \text{Eu}^{3+}$ series, the $\text{Eu}^{3+} : ^5\text{D}_0 - ^7\text{F}_0$ energies at the C_2 site of C-type RE_2O_3 for RE = Gd, Y, and Lu²⁰ and at the C_{3v} site of A-type La_2O_3 ²¹ are shown. The $\text{Eu}^{3+} : ^5\text{D}_0 - ^7\text{F}_0$ energy shifts to lower energy with decreasing RE ionic radius in the $\text{RE}_2\text{O}_2\text{S}$ hosts, whereas for $\text{RE}_2\text{O}_3 : \text{Eu}^{3+}$, the energy remains fairly constant. Generally, the 4f–4f transition energy can be affected by both the crystal field^{22,23} and the nephelauxetic effect.^{24–26} Because $\text{Eu}^{3+} : ^5\text{D}_0 - ^7\text{F}_0$ does not show any luminescence lines related to the Stark splitting, $\text{Eu}^{3+} : ^5\text{D}_0 - ^7\text{F}_0$ reflects only the nephelauxetic effect. Also, in the series of $\text{RE}_2\text{O}_2\text{S}$ with the same crystal structure, the Eu^{3+} luminescence energy can be shifted to lower energy mainly by enhancing the nephelauxetic effect. This is probably because of the unique crystal structure of $\text{RE}_2\text{O}_2\text{S}$ and the small electronegativity of S^{2-} . The $\text{RE}_2\text{O}_2\text{S}$ crystal forms a layered structure by S^{2-} , O^{2-} , and RE^{3+} sheets, and the RE site is asymmetrically coordinated by four O^{2-} and three S^{2-} , as shown in Figure 10. For this asymmetric coordination, the 4f electron cloud can be expanded to the S^{2-} ions because of the smaller electronegativity than oxide ($\chi_{\text{S}} = 2.58 < \chi_{\text{O}} = 3.44$). This unique crystal structure and the smaller RE site may lead to an increase in the nephelauxetic effect. This strong nephelauxetic effect for Eu^{3+} applies equally well to all other Ln³⁺ ions. From the host compound dependence of

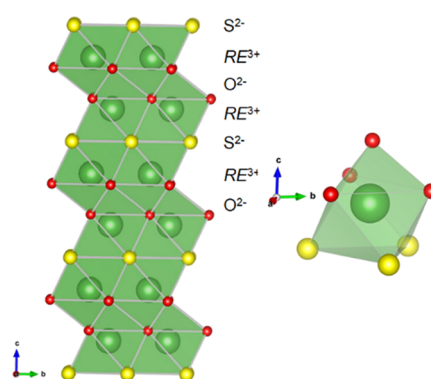


Figure 10. Crystal structure of $\text{RE}_2\text{O}_2\text{S}$ (the crystal structure is drawn by VESTA software²⁷).

the hole trap difference between Pr^{3+} and Tb^{3+} and the Eu^{3+} luminescence red-shifting, the decreasing β parameter in the order of $\text{La}_2\text{O}_2\text{S}$, $\text{Gd}_2\text{O}_2\text{S}$, $\text{Y}_2\text{O}_2\text{S}$, and $\text{Lu}_2\text{O}_2\text{S}$ appears consistent and reasonable.

4.4. Construction of the VRBE Diagram Considering the Nephelauxetic Effect. Based on the observed trap depth variation of Pr^{3+} and Tb^{3+} in $\text{RE}_2\text{O}_2\text{S}$, new VRBE diagrams that take the nephelauxetic effect into account need to be constructed. To make a new VRBE diagram, the required energetic parameters were also updated based on the newly obtained spectroscopic data. They are compiled in Table 3. The exciton creation energy was determined from the PLE from the VUV to UV range at 15 K (Figure S1 in the Supporting Information) as treated in Section 3.2. To obtain the CT energies, the PLE spectra in the energy scale from Figure 2 were deconvoluted by two Gaussian peaks because we assumed CT absorption both from O^{2-} and from S^{2-} . For example, two clear PLE bands can be seen in Figure 2a for $\text{Lu}_2\text{O}_2\text{S} : \text{Eu}^{3+}$. The electronegativity of S is smaller than that of O, forming the top of the valence state by the 3p orbital of S. Thus, the lower CT energies were used for the VRBE diagram. The red-shift parameter of Ce^{3+} was calculated using the 4f–5d₁ absorption peak reported in ref 28. The $U(6, A)$ value of $\text{RE}_2\text{O}_2\text{S}$ is reported to be around 6.37 eV.⁷ $U(6, A)$ is the energy difference between the VRBE of Eu^{2+} and Eu^{3+} and it depends on the screening distance in the chemical shift model.²⁹ In this study, we also adopted a $U(6, A)$ value of 6.37 eV.⁷

Figure 11 shows the new VRBE diagram for $\text{La}_2\text{O}_2\text{S}$ using the updated parameters. Different from the previous VRBE diagram, the VRBE of Tb^{3+} is located slightly below that of Pr^{3+} . The electron trap depth by Eu^{3+} is 1.21 eV, and the hole trap depths by Pr^{3+} and Tb^{3+} are 0.78 and 0.75 eV, respectively. Because the hole trap depth by Pr^{3+} and Tb^{3+} is smaller than the electron trap depth by Eu^{3+} , the hole trap is released at a lower temperature than the electron trap. Thus, the VRBE diagram also supports the hole detrapping mechanisms for persistent luminescence.

Figure 12 shows a stacked VRBE diagram of $\text{RE}_2\text{O}_2\text{S}$. In the new VRBE diagram, the observed unusual trend of hole trap depth (the deepest in $\text{La}_2\text{O}_2\text{S}$ and the shallowest in $\text{Lu}_2\text{O}_2\text{S}$) can be explained partly. The energy difference between the top of VB and Ln³⁺ (Pr^{3+} , Tb^{3+}) in $\text{La}_2\text{O}_2\text{S}$ is much larger than that in $\text{Lu}_2\text{O}_2\text{S}$. Figure 13 summarizes the hole trap depth by Pr^{3+} and Tb^{3+} estimated from the experimental results and the VRBE diagram. The VRBE diagram cannot explain the hole

Table 3. Parameters and Spectroscopic Data Utilized to Construct the VRBE Diagram of Ln in the RE₂O₂S Host and the Estimated VRBE Values in the eV Unit (Except for the Nephelauxetic Ratio β)^{a,b}

| | $U(6,A)$ ⁷ | E^{ex} | E^{CT} | β | $D(1,3+A)$ | E_V | E_C | $E_{\text{Eu}^{2+}}$ | $E_{\text{Pr}^{3+}}$ | $E_{\text{Tb}^{3+}}$ |
|----------------------------------|-----------------------|-----------------|-----------------|---------|------------|-------|-------|----------------------|----------------------|----------------------|
| La ₂ O ₂ S | 6.37 | 4.62 | 3.58 | 0.930 | 3.39 | -7.34 | -2.72 | -3.77 | -6.64 | -6.67 |
| Gd ₂ O ₂ S | 6.37 | 4.66 | 3.60 | 0.927 | 3.45 | -7.43 | -2.77 | -3.75 | -6.57 | -6.63 |
| Y ₂ O ₂ S | 6.37 | 4.81 | 3.58 | 0.927 | 3.44 | -7.37 | -2.56 | -3.77 | -6.63 | -6.68 |
| Lu ₂ O ₂ S | 6.37 | 4.82 | 3.56 | 0.924 | 3.45 | -7.34 | -2.52 | -3.78 | -6.67 | -6.75 |

^aThe method of refs 12 and 13 was followed. ^b $U(6,A)$: energy difference between the VRBE of Eu²⁺ and Eu³⁺ in host A, E^{ex} : host exciton creation energy, E^{CT} : charge transfer energy from the anion to Eu³⁺, β : nephelauxetic ratio, $D(1,3+A)$: energy difference between the quasi-free ion 4f–5d energy and the observed 4f–5d energy of Ce³⁺ in host A, E_V , E_C , $E_{\text{Eu}^{2+}}$, $E_{\text{Pr}^{3+}}$, and $E_{\text{Tb}^{3+}}$: VRBE of the valence band top, conduction band bottom, Eu²⁺, Pr³⁺, and Tb³⁺, respectively.

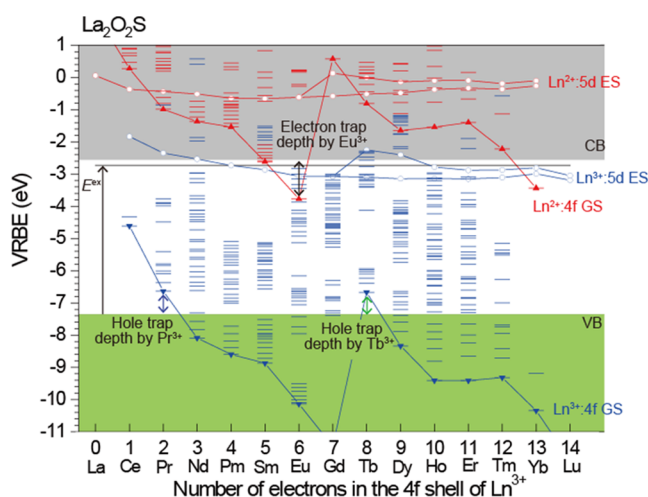


Figure 11. VRBE diagram of La₂O₂S. VB: valence band, CB: conduction band, GS: ground state, ES: excited state, and Ln: lanthanide ions.

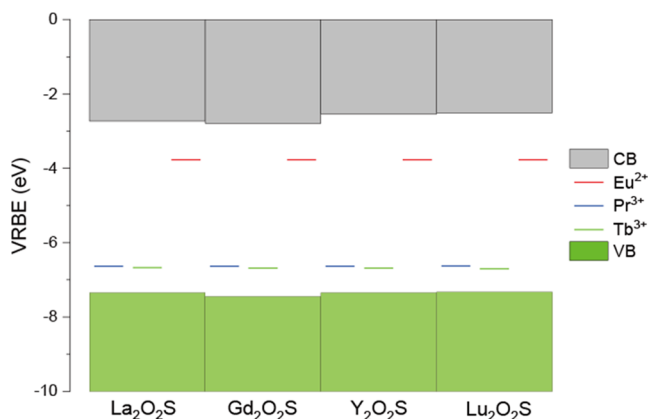


Figure 12. Stacked VRBE diagram of RE₂O₂S with the ground state of Eu²⁺, Pr³⁺, and Tb³⁺.

trap depth in Gd₂O₂S, but it can explain the decreasing trend of hole trap depth from La to Lu. For this trend, La₂O₂S:Eu³⁺–Ln³⁺ shows the deep trap depth among the RE₂O₂S hosts and it is closest to ambient temperature. For the application demanding a longer persistent duration, La₂O₂S:Eu³⁺–Ln³⁺ is not suitable. However, the strong red persistent luminescence in a short time range (>100 mcd/m² for a few seconds) for La₂O₂S:Eu³⁺–Pr³⁺ can be used as security ink and so on.

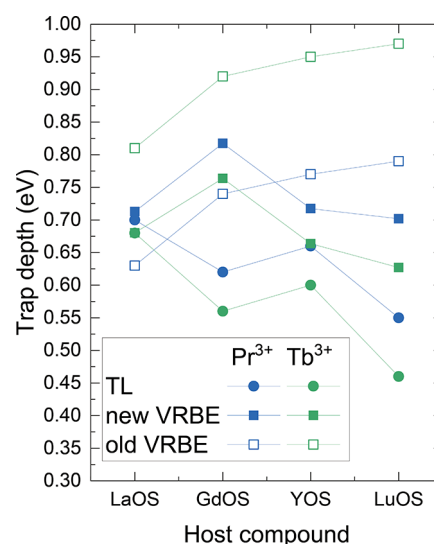


Figure 13. Hole trap depths of Pr³⁺ and Tb³⁺ estimated from the TL glow peak and from the reported VRBE diagram⁵ and the newly constructed VRBE diagram.

5. CONCLUSIONS

Red RE₂O₂S:Eu³⁺–Ln³⁺ (RE = La, Gd, Y, Lu; Ln = Pr, Tb) thermoluminescence phosphors were developed, where Pr³⁺ and Tb³⁺ codoping generated additional TL glow peaks. Persistent luminescence and thermoluminescence have been identified to arise from only Eu³⁺. Eu³⁺ persistent luminescence appears after excitation in the charge transfer band of Eu³⁺ and by means of band-to-band excitation. Based on the obtained results, it was concluded that the persistent luminescence of Eu³⁺ is caused by the hole trapping at Pr³⁺ and Tb³⁺ followed by a thermal detrapping process. The vacuum referred binding energy diagrams of RE₂O₂S taking into account the nephelauxetic effect were constructed. Using a new VRBE diagram, the deeper hole trap of Pr³⁺ than that of Tb³⁺ was explained by a right-hand branch lowering of the zig-zag curve of Ln³⁺ due to an enhanced nephelauxetic effect caused by sulfide ions. This is consistent with an observed red-shifting of the Eu³⁺ emission lines. The hole trap depth tendency of Pr³⁺ and Tb³⁺ with respect to different hosts of RE₂O₂S except for Gd₂O₂S was understood by a new VRBE diagram. La₂O₂S:Eu³⁺–Pr³⁺ is the best composition among the samples for a persistent phosphor at ambient temperature, showing strong red persistent luminescence in a short time range (>100 mcd/m² for a few seconds).

■ ASSOCIATED CONTENT

SI Supporting Information

The Supporting Information is available free of charge at <https://pubs.acs.org/doi/10.1021/acs.jpcc.3c03251>.

PLE in the vacuum UV region and TL glow curves (PDF)

■ AUTHOR INFORMATION

Corresponding Author

Jumpei Ueda – Graduate School of Advanced Science and Technology, Japan Advanced Institute of Science and Technology, 923-1292 Ishikawa, Japan; Graduate School of Human and Environmental Studies, Kyoto University, 606-8501 Kyoto, Japan; orcid.org/0000-0002-7013-9708; Email: ueda-j@jaist.ac.jp

Authors

Atsunori Hashimoto – Graduate School of Advanced Science and Technology, Japan Advanced Institute of Science and Technology, 923-1292 Ishikawa, Japan; NEMOTO & CO., LTD, Hiratsuka 254-0076 Kanagawa, Japan

Yasushi Aoki – NEMOTO & CO., LTD, Hiratsuka 254-0076 Kanagawa, Japan

Pieter Dorenbos – Faculty of Applied Sciences, Delft University of Technology, 2629 JB Delft, The Netherlands

Setsuhisa Tanabe – Graduate School of Human and Environmental Studies, Kyoto University, 606-8501 Kyoto, Japan; orcid.org/0000-0002-7620-0119

Complete contact information is available at:

<https://pubs.acs.org/doi/10.1021/acs.jpcc.3c03251>

Author Contributions

[†]A.H. and J.U. contributed equally. J.U. conceived the idea of the study. A.H. and Y.A. prepared the materials. J.U. and A.H. investigated the structure properties and optical properties. A.H., J.U., and P.D. constructed the energy diagrams. A.H. and J.U. drafted the original manuscript. J.U. and S.T. supervised the conduct of this study. All authors reviewed the manuscript draft and revised it critically on intellectual content. All authors approved the final version of the manuscript to be published.

Notes

The authors declare no competing financial interest.

■ ACKNOWLEDGMENTS

This research was financially supported by JSPS KAKENHI (grant number 18KK0405, 20H02438).

■ REFERENCES

- (1) Xu, J.; Tanabe, S. Persistent luminescence instead of phosphorescence: History, mechanism, and perspective. *J. Lumin.* **2019**, *205*, 581–620.
- (2) Ueda, J. How to Design and Analyze Persistent Phosphors? *Bull. Chem. Soc. Jpn.* **2021**, *94*, 2807–2821.
- (3) Matsuzawa, T.; Aoki, Y.; Takeuchi, N.; Murayama, Y. A new long phosphorescent phosphor with high brightness, SrAl₂O₄:Eu²⁺, Dy³⁺. *J. Electrochem. Soc.* **1996**, *143*, 2670–2673.
- (4) Dorenbos, P. Mechanism of persistent luminescence in Eu²⁺ and Dy³⁺ codoped aluminate and silicate compounds. *J. Electrochem. Soc.* **2005**, *152*, H107.
- (5) Joos, J. J.; Korthout, K.; Amidani, L.; Glatzel, P.; Poelman, D.; Smet, P. F. Identification of Dy³⁺/Dy²⁺ as Electron Trap in Persistent Phosphors. *Phys. Rev. Lett.* **2020**, *125*, No. 033001.

(6) Murazaki, Y.; Arai, K.; Ichinomiya, K. New Red Long Persistence Phosphor. *J. Illum. Engng. Inst. Jpn.* **1999**, *83*, 445–446.

(7) Luo, H.; Bos, A. J. J.; Dorenbos, P. Charge Carrier Trapping Processes in RE₂O₂S (RE = La, Gd, Y, and Lu). *J. Phys. Chem. C* **2017**, *121*, 8760–8769.

(8) Lin, F.; Li, X.; Chen, C.; Pan, X.; Peng, D.; Luo, H.; Jin, L.; Zhuang, Y.; Xie, R.-J. Modeling Polyhedron Distortion for Mechanoluminescence in Mixed-Anion Compounds RE₂O₂S:Ln³⁺. *Chem. Mater.* **2022**, *34*, 5311–5319.

(9) Randall, J. T.; Wilkins, M. H. F. Phosphorescence and Electron Traps. II. The Interpretation of Long-Period Phosphorescence. *Proc. Roy. Soc. A Math. Phys. Sci.* **1945**, *184*, 390–407.

(10) Randall, J. T.; Wilkins, M. H. F. Phosphorescence and Electron Traps. I. The Study of Trap Distributions. *Proc. Roy. Soc. A Math. Phys. Sci.* **1945**, *184*, 365–389.

(11) Bos, A. J. J. Theory of Thermoluminescence. *Rad. Meas.* **2006**, *41*, S45–S56.

(12) Yokono, S.; Imanaga, S.; Hoshina, T. Raman Spectra for Eu Doped Ln₂O₂S Phosphors. *J. Phys. Soc. Jpn.* **1979**, *46*, 1882–1888.

(13) Dorenbos, P. The hole picture as alternative for the common electron picture to describe hole trapping and luminescence quenching. *J. Lumin.* **2018**, *197*, 62–65.

(14) Dorenbos, P.; Bos, A. J. J.; Poolton, N. R. J. Carrier recombination processes and divalent lanthanide spectroscopy in YPO₄:Ce³⁺;L³⁺ (L = Sm, Dy, Tm). *Phys. Rev. B* **2010**, *82*, 195127.

(15) Korthout, K.; Van den Eeckhout, K.; Botterman, J.; Nikitenko, S.; Poelman, D.; Smet, P. F. Luminescence and x-ray absorption measurements of persistent SrAl₂O₄:Eu, Dy powders: Evidence for valence state changes. *Phys. Rev. B* **2011**, *84*, No. 085140.

(16) Ueda, J.; Katayama, M.; Asami, K.; Xu, J.; Inada, Y.; Tanabe, S. Evidence of valence state change of Ce³⁺ and Cr³⁺ during UV charging process in Y₃Al₂Ga₃O₁₂ persistent phosphors. *Opt. Mater. Express* **2017**, *7*, 2471–2476.

(17) Ueda, J.; Xu, J.; Takemura, S.; Nakanishi, T.; Miyano, S.; Segawa, H.; Tanabe, S. How Many Electron Traps are formed in Persistent Phosphors? *ECS J. Solid. State Sci. Technol.* **2021**, *10*, No. 116003.

(18) Dorenbos, P. The nephelauxetic effect on the electron binding energy in the 4fⁿ ground state of lanthanides in compounds. *J. Lumin.* **2019**, *214*, No. 116536.

(19) Dorenbos, P. [INVITED] Improved parameters for the lanthanide 4fⁿ and 4fⁿ⁻¹5d curves in HRBE and VRBE schemes that takes the nephelauxetic effect into account. *J. Lumin.* **2020**, *222*, No. 117164.

(20) Malta, O. L.; Antic-Fidancev, E.; Lemaitre-Blaise, M.; Milicic-Tang, A.; Taibi, M. The crystal field strength parameter and the maximum splitting of the ⁷F₁ manifold of the Eu³⁺ ion in oxides. *J. Alloys Compd.* **1995**, *228*, 41–44.

(21) Moune, O. K.; Porcher, P.; Caro, P. A new analysis of the fluorescence spectrum of Eu³⁺ in A-type La₂O₃. *J. Solid State Chem.* **1983**, *50*, 41–50.

(22) Antic-Fidancev, E.; Hölsä, J.; Lastusaari, M.; Lupei, A. Dopant-host relationships in rare-earth oxides and garnets doped with trivalent rare-earth ions. *Phys. Rev. B* **2001**, *64*, No. 195108.

(23) Tanner, P. A.; Yeung, Y. Y.; Ning, L. What Factors Affect the ⁵D₀ Energy of Eu³⁺? An Investigation of Nephelauxetic Effects. *J. Phys. Chem. A* **2013**, *117*, 2771–2781.

(24) Frey, S. T.; Horrocks, W. D. On correlating the frequency of the ⁷F₀ → ⁵D₀ transition in Eu³⁺ complexes with the sum of 'nephelauxetic parameters' for all of the coordinating atoms. *Inorg. Chim. Acta* **1995**, *229*, 383–390.

(25) Albin, M.; Horrocks, W. D. Europium(III) luminescence excitation spectroscopy. Quantitative correlation between the total charge on the ligands and the ⁷F₀ → ⁵D₀ transition frequency in europium(III) complexes. *Inorg. Chem.* **1985**, *24*, 895–900.

(26) Caro, P.; Beaury, O.; Antic, E. L'effet néphélauxétique pour les configurations 4fⁿ en phase solide. *J. Phys. France* **1976**, *37*, 671–676.

(27) Momma, K.; Izumi, F. VESTA 3 for three-dimensional visualization of crystal, volumetric and morphology data. *J. Appl. Crystallogr.* **2011**, *44*, 1272–1276.

(28) Yokono, S.; Abe, T.; Hoshina, T. Red luminescence of Ce³⁺ due to the large Stokes shifts in Y₂O₃S and Lu₂O₃S. *J. Lumin.* **1981**, *24–25*, 309–312.

(29) Dorenbos, P. Modeling the chemical shift of lanthanide 4f electron binding energies. *Phys. Rev. B* **2012**, *85*, No. 165107.

Recommended by ACS

Site-Selective Eu³⁺ Doping and Enhanced Luminescence from Eu³⁺ at B Sites in Perovskite-Type Strontium Zirconate and Hafnate

Kazushige Ueda, Tetsuo Honma, *et al.*

JULY 28, 2023

THE JOURNAL OF PHYSICAL CHEMISTRY C

READ 

Making Eu²⁺- and Sm²⁺-Doped Borates Fit for Solar Energy Applications

L. J. B. Erasmus, H. C. Swart, *et al.*

MARCH 01, 2023

ACS PHOTONICS

READ 

Enhancement of the NIR Emission of Cr³⁺–Yb³⁺ Co-doped La₃GaGe₅O₁₆ Phosphors by Doping Nd³⁺ Ions via Efficient Energy Transfer for NIR Spectroscopy Regulation

Feiyue Fan, Lei Zhao, *et al.*

AUGUST 16, 2022

INORGANIC CHEMISTRY

READ 

Ultra-broad Near-Infrared Emitting Phosphor LiInF₄: Cr³⁺ with Extremely Weak Crystal Field

Liping Song, Haomiao Zhu, *et al.*

JULY 03, 2023

INORGANIC CHEMISTRY

READ 

Get More Suggestions >